Journal of Marine Science and Technology, Vol. 25, No. 5, pp. 520-530 (2017)
DOI: 10.6119/JMST-017-0504-1

HYDRODYNAMIC PERFORMANCE OF AN OSCILLATING WAVE SURGE CONVERTER IN REGULAR AND IRREGULAR WAVES: AN EXPERIMENTAL STUDY

Dezhi Ning[1], Chengguo Liu[1], Chongwei Zhang[1],
Malin Göteman[2], Haitao Zhao[3], and Bin Teng[1]

Key words: oscillating wave surge converter, bottom-hinged flap-type device, CWR, physical experiment, hydrodynamic performance.

ABSTRACT

A series of physical experiments are carried out to investigate the hydrodynamic performance of a bottom-hinged flap-type oscillating wave surge converter (OWSC). The power take-off (PTO) system in the OWSC is achieved with the magnetic powder brake. Both regular and irregular wave conditions are considered. It is observed that the capture width ratio (CWR) of the proposed OWSC is strongly affected by the PTO damping torque, incident wave amplitude, inertia of the structure and wave spectrum etc.

I. INTRODUCTION

Due to the excessive use of fossil fuels, the concerns of climate change have motivated the increased global interest in the extraction of energy from renewable sources. The ocean is a huge renewable energy source, which could make a significant contribution to the world's energy supply. However, no current technology has demonstrated that energy could be extracted from ocean waves at an economic and efficient way (Folley et al., 2007(a)). Further study is necessary to provide the scientific evidence for the effectiveness of wave energy converters (WECs).

Up to now, the majority of effort has been put in the investigation of shoreline oscillating water columns (OWC) and offshore floating devices. Shoreline OWC has attracted more interest because of the fundamental simplicity of operation and good accessibility. Offshore floating devices are normally operated in deep water where higher levels of annual average incident wave power are expected. However, the seabed-mounted nearshore devices have received less focus so far, due to a traditional opinion that the wave power resource in nearshore region is dramatically less than that in offshore. In fact, the work in (Folley and Whittaker, 2009; Folley et al., 2009; Whittaker and Folley, 2012) revealed that the exploitable wave power resource in nearshore region is only 10-20% less than that in offshore. Nevertheless, with the consideration of many influencing factors, such as economy, engineering difficulty, survivability etc., to build wave energy farms in the nearshore region is very competitive.

Many analytical and numerical works on the hydrodynamic performance of flap-type WEC devices have been published. Penney and Price (1952) analytically studied an isolated three-dimensional surface-piercing plate with negligible thickness in waves and derived an approximate diffraction solution. Folley et al. (2007a) numerically studied the effect of water depth on the performance of a small surging energy converter and showed that the power capture was much related to the incident wave force rather than the incident wave power. They demonstrated that both the surge wave force and power capture of a flap-type wave energy converter increase with the decrease of water depth. Folley et al. (2007b) developed a linearized frequency domain numerical model for studying a small seabed-mounted bottom-hinged flap-type wave energy converter to account for vortex shedding at body edges and decoupling at large rotational angles. The results indicated that in general the capture factor increases with both the device width and wave frequency due to increasing wave force. However, shallower water and smaller incident wave were not considered in their study. Babarit et al. (2012) numerically simulated the performance of various wave energy conversion devices including the bottom-hinged flap-type

Paper submitted 07/12/16; revised 11/21/16; accepted 05/04/17. Author for correspondence: Dezhi Ning (e-mail: dzning@dlut.edu.cn).
[1] *State Key Laboratory of Coastal and Offshore Engineering, Dalian University of Technology, Dalian, China.*
[2] *Department of Engineering Science, University of Uppsala, Uppsala, Sweden.*
[3] *Institute of Hydraulic & Environmental Engineering, Zhejiang University of Water Resources and Electric Power, Hangzhou, China.*

wave energy converter. A numerical study on the hydrodynamics of bottom-hinged plate wave energy converters in regular and irregular waves was performed by (Gomes et al., 2015). Renzi and Dias (2012), Renzi and Dias (2013) have developed a mathematical model based on potential flow theory to investigate the behavior of the bottom-hinged flap-type WEC in a channel and in the open ocean, respectively. Then they applied this approach to mathematically explain the physical operating principles of flap-type WEC (Renzi et al., 2014). Meanwhile, they indicated that the power absorption and performance of the OWSC device were driven by the exciting torque and the natural period of the OWSC device was much larger than the torque peak period. Then the optimal capture width ration may be attained around the torque peak period which is apart from the natural period of the OWSC device. Folley et al. (2007b), Fitzgerald and Bergdahl (2009) claimed that viscous effects might result in a considerable reduction of power capture, especially nearby the resonance. So it is meaningful to avoid the OWSC working in the states of nearby the resonance for which can result in a larger rotational response and a stronger viscous effect. That is not only unfavorable for power capture but also a severe threat to the safe operation of the device. Then increasing attention has been paid to study the hydrodynamic performance of the OWSC device in normal sea states. Wei et al. (2015), Wei et al. (2016) performed experimental and numerical studies of wave interactions with an oscillating wave surge converter, which were focused on two aspects, i.e., viscous effect on the device performance under normal operating conditions and slamming effect on the device survivability under extreme conditions. They suggested that the diffraction/radiation effects dominate the device motion. The viscous effects are negligible for wide flaps and slamming on an oscillating flap is the result of the strong coupling between the incident waves and the flap motion.

Due to the fact that most analytical and numerical works were based on linear potential theory, many experimental works have also been conducted to investigate the hydrodynamic performance of the WEC device in more realistic conditions. A bottom-pivoted pitching cylinder for wave energy conversion was experimentally studied by Caska and Finnigan (2008). It was found that the non-linear drag term has a significant effect on the performance of energy converters. But it was often neglected in the study of wave energy conversion. Laboratory experiments of the pitching vertical cylinder in a wave flume were carried out by Flocard and Finnigan (2010), Flocard and Finnigan (2012). They found that both damping and ballasting dramatically affect the performance of the device. Moreover, it was shown that these parameters could be adjusted in response to the wave conditions to optimize power capture. Sheng et al. (2015) carried out a study on the different type of power take-off (PTO) damping (i.e., *linear and nonlinear*) and their optimizations for maximizing wave energy conversions on a point absorber wave energy converter.

As it better represents real ocean conditions, the study on the performance of WECs in irregular waves is of immense importance. The wave spectrum plays a significant role in the energy transfer, and the effects of spectral characteristics on the efficiency have been investigated by many researchers. Saulnier et al. (2007) numerically investigated the dependency of wave energy conversion on the spectral bandwidth of sea-states for an axisymmetric wave energy converter. Clabby et al. (2012) carried out an experimental analysis to investigate the effect of the spectral distribution of wave energy on the performance of the device. Sarkar et al. (2013) experimentally investigated the behavior of a bottom-hinged flap-type wave energy converter in random seas and observed that the oscillating wave energy converter with larger width captures larger power for all random seas tested.

However, the related experimental studies on bottom-hinged flap-type OWSC devices are still limited, especially those on the influence of PTO damping torque, mass distribution and wave states on the hydrodynamic performance of the OWSC device. Hughes (1996) stated that though experimental testing of small scale models in waves flumes was an efficient way to investigate the hydrodynamic performance of the model, laboratory effects due for example to the wave reflection and blockage effects may affect the results. Hence, more attention has to be paid to understand and optimize the performance of flap-type OWSC devices in realistic conditions. To complete the previous studies, the primary goal of this study is to experimentally investigate the effects of PTO damping (i.e., *the approximately coulomb damping force of power take-off system considered*), wave amplitude and three different mass distributions on the bottom-hinged OWSC devices. Besides, the effects of wave states on the hydrodynamic performance are also investigated in this study.

In the present study, a parametric study of the hydrodynamic performance of the proposed wave energy converter under regular and irregular waves is performed. The variations of the CWR (capture width ratio) as function of the PTO damping force can be obtained for different parameters including wave conditions and mass distribution. The rest of the paper is organized as follows. The experimental description is given in Section 2. The uncertainty analysis and theoretical calculation method of capture width ratio is presented in Section 3. Section 4 presents the performance of the OWSC device in regular waves for different typical incident waves and mass distributions, and in irregular waves for different wave spectra. Finally, the conclusions are summarized in Section 5.

II. EXPERIMENTAL DESCRIPTION

The experiments were conducted in a wave flume at the State Key Laboratory of Coastal and Offshore Engineering, Dalian University of Technology, China. The flume is 60 m long, 4.0 m wide and 2.5 m deep. A piston-type unidirectional wave-maker was installed at one end of the flume, and a wave-absorbing beach was located at the other end to dissipate the outgoing waves. The model was positioned on the central line of the wave flume with a distance of 40 m from the wave maker, as shown in Fig. 1.

The full-scale device is designed for the water depth of 5.0 m.

Table 1. Parameters of the model for the three mass distributions.

	No B	1B	2B
Mass (kg)	29.80	51.80	73.40
Inertia (kg · m^2)	13.77	14.52	17.81
Natural period (s)	4.2	4.8	5.8
Natural frequency (rad/s)	1.50	1.31	1.08
Mass center (m)	-0.315	-0.423	-0.432

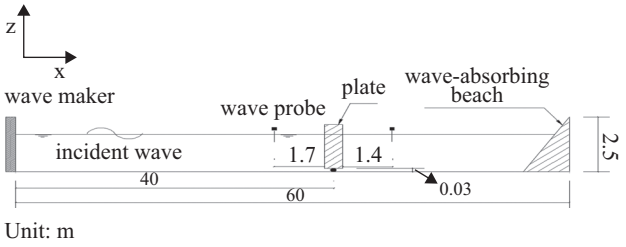

Fig. 1. Schematic of the experiment (unit: m).

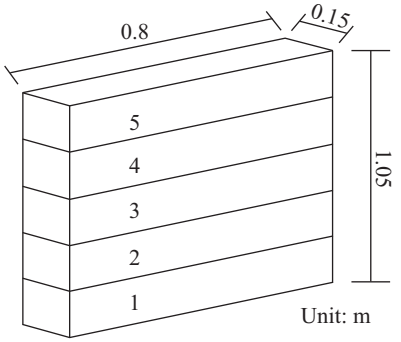

Fig. 2. Bottom-hinged plate and its dimensions (unit: m).

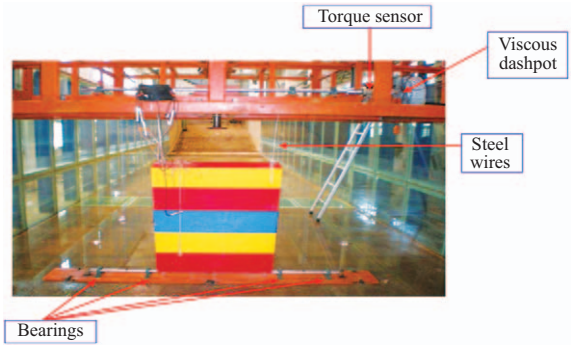

Fig. 3. Picture of the arrangement in the wave flume.

The full-scale wave period and amplitude vary from 2.1 s to 7.5 s and from 0.135 m to 0.415 m, respectively. Since gravitational effects are predominant over the factors such as roughness, viscosity and surface tension, Froude scaling is used to infer prototype results. In the present experiments, a 1:5 scale model is used in the experiment, and the water depth is set as 0.9 m. The basic structural parameters (i.e., *width D, height d and thickness t*) of the buoyant plate can be seen in Fig. 2. The WEC model composes five chambers into which water can be pumped so that different mass distribution can be achieved. To avoid the sloshing influence, the considered chamber is fully filled with water. For all the tests mentioned in this paper, the symbol '1B' means that the first bottom chamber (i.e., *the lowest one*) is fully filled with water, '2B' the two bottom chambers fully filled with water, and 'No B' all the chambers being empty. The modification of inertia due to the ballasting results in a change in the natural frequency of the device (*which can be obtained in the free decay tests as shown in Fig. A, in the Appendix*), as shown in Table 1.

The plate is anchored on the flume floor with the static water depth $h = 0.9$ m and allows to undergo pitch motion around the y axis normal to the wave direction, which means that the angular position of the plate is zero when the plate is in the equilibrium vertical position. The x axis is defined along the direction of wave propagation, the y axis is perpendicular to the wave flume, and the z axis is vertical upward measured from the still water surface. The wave elevations are recorded by two wave probes (i.e., *one located 1.7 m ahead of the plate and the other located 1.4 m behind the plate*) and the precisions of the present measurement instruments is ±0.1 cm for the wave height. The measured period is obtained by the method of the up crossing zero point and down crossing zero point in the time series of wave elevation. The measured wave amplitude is the average value of the difference of adjacent crest and trough values (i.e., *the time-series data of wave gauges and descriptions of how to compute the wave heights and periods from the data are shown in Fig. B, in the Appendix*). To ensure the reliability of the experimental data, each case is repeated three times.

The bottom of the plate is attached to a 0.03 m-diameter bottom shaft which is fixed on the flume bottom by the low friction bearings. The other rotating shaft is fixed on the top of the wave flume. The two shafts are matched through two pre-tensioned stainless steel wires combined with two pairs of bearings. The PTO system consists of a magnetic powder brake (i.e., *the model type of the magnetic powder brake is ZZ-20 and the precisions of the present measurement instruments is* ±0.5% *Nm for the PTO's torque.*), which is expected to produce different Coulomb damping force or approximate Coulomb damping force, and a current controller (i.e., *the model type of the current controller is WLY-3A and the precisions of the present measurement instruments is* ±1.5% *for the magnetizing current*). The PTO damping force can be set by adjusting the current by the current

Table 2. Wave parameters and test conditions in the experiments.

T (s)	0.94	1.16	1.30	1.79	2.24	3.13	
A_i (m)	0.027	0.04	0.05	0.083	0.067	0.067	
I (A)	0.0	0.1	0.2	0.3	0.4	0.5	0.6
Mass distribution	No B	1B	2B				

Table 3. Wave parameters and test conditions in the case of No B.

T (s)	1.30	2.24
Ai (m)	0.034 0.043 0.056 0.064	0.045 0.056 0.075 0.083
I (A)	0.0 0.2 0.4 0.6	

Table 4. Test conditions of No B for JONSWAP and PM spectra.

T_e (s)	1.30	2.24			
H_s (m)	0.068	0.10	0.128	0.132	0.176
I (A)	0.0	0.1	0.3	0.5	

Note: T_e means the average wave period and H_s is the significant wave height in an irregular wave group.

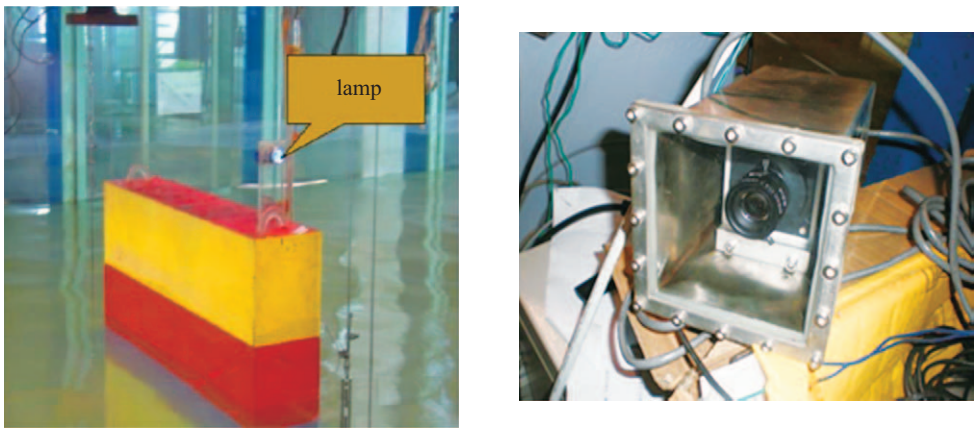

Fig. 4. Picture of the high-speed CCD camera and angular encoder.

controller, which is connected to a magnetic powder brake. The magnetizing current controller (i.e., *magnetic powder brake system*) is installed on the top of wave flume and connected to the upper shaft. A torque sensor, which is expected to measure the PTO torque (*i.e., the time histories of PTO torque is shown in Fig. C, in the Appendix*), is connected with the magnetic powder brake (*i.e., the output damping torque of the magnetic powder brake system is shown in Table a, in the Appendix*), as shown in Fig. 3.

The non-contact displacement measurement system comprises a high-speed CCD camera and a laser lamp which is fixed on the WEC model. The maximum shooting speed of the CCD high-speed camera is 200 frames per second. Through the analysis of the continuous recording of the motion of the laser lamp, the pivot angle and rotational response (i.e., *which is determined as shown in Fig. D in the Appendix*) of the WEC can be obtained, as shown in Fig. 4.

And total four series of tests are considered in the present study. For the first two series of tests, the wave period varies from 0.94 s to 3.13 s, and the magnetizing current varies from 0.0 A to 0.6 A, see Table 2. Tests of three kinds of mass distribution, which can be realized by adjusting the amount of ballast in the lowest chambers of the device, are performed for the third test. Finally, the effect of different irregular waves is evaluated with two spectra and the effects of different wave states are tested. The corresponding test conditions are presented in Tables 2-4.

III. UNCERTAINTY ANALYSIS AND THEORETICAL CALCULATION METHOD OF CAPTURE WIDTH RATIO

Free decay experiments are firstly performed to measure the nature frequency of the device. From the histories of the rotation angle in Fig. A, it can be found that the natural frequencies

are 1.50 rad/s for case No B, 1.31 rad/s for case 1B, and 1.08 rad/s for case 2B. To approximate the error range of this measurement, the analytical solution for the natural frequency is further derived for comparison.

For a bottom-hinged OWSC, the natural frequency ω_n is a function of the ratio of the buoyancy term to the total inertia:

$$\omega_n = \sqrt{\frac{C}{I_1 + I_a}} \tag{1}$$

$$I = \frac{\rho_s tDd(t^2 + 4d^2)}{12} = \frac{\rho_s tDd^3((\frac{t}{d})^2 + 4)}{12} \tag{2}$$

$$C = \frac{\rho g t^3 D}{12} + \frac{(\rho - \rho_s) g t D d^2}{2} \tag{3}$$

$$I_a = \frac{M_w h^2}{3} = \frac{\rho t D h^3}{3} \tag{4}$$

where I_1 is moment of inertia of the device, I_a is the frequency dependent added moment inertia and C is the hydrostatic restoring coefficient, ρ is the water density, ρ_s is the structure density, g is the gravity acceleration, M_w is the mass of displaced water. For simplicity, the expression for natural frequency can be simplified as follows

$$\omega_n = \sqrt{\frac{3g(\rho - \rho_s)}{2h(\rho + \rho_s)}} \tag{5}$$

From this equation, it is known that the analytical solutions of the natural frequencies are 1.38 rad/s for case No B, 1.17 rad/s for case 1B, and 1.00 rad/s for case 2B. Therefore, compared with the analytical solution, the relative error of measurement is 8.6% for case No B, 12% for case 1B and 8% for case 2B.

Another consideration in terms of the measurement accuracy is about the magnetic powder brake system. In the present experiment, due to irregular disturbance, the output damping force does not strictly satisfy the theoretical setup. Fig. C is a typical example, which compares the measured and theoretical damping torques in the wave condition of $T = 3.13$ s and $A_i = 0.067$ m. It can be seen that the measured results are not exactly the same as the theoretical value. In this study, the error is analyzed as follows:

$$\Delta = \frac{\sqrt{\sum((|T_1| - |T_2|) * 0.02)}}{|T_1|} \tag{6}$$

where T_1 is the theoretical damping torque, T_2 is the measured damping torque, and Δ is the relate error. Thus, the relate error is 0.3 for the case of $T_{pto} = 37.5$ Nm and 0.2 for the case of $T_{pto} = 75$ Nm.

It should be noted that, in this experiment, the torque is transmitted from the bottom to upper shaft through pre-tensioned stainless steel wire. Since the shaft motion is bi-directional with a slack side of the wire, some torque may be absorbed by the wire. So the torque indirectly measured in this study may be smaller than the 'real' torque. However, we believe that the energy dissipation in this process may only be significant for some extreme situations. So this torque offset is not specially analyzed in details in this study. Because of the existence of irregular disturbance, the time history of the measured torque is not strictly significant in Coulomb damping. Therefore, using an approximation to replace the Coulomb damping is desirable. Power capture here represents the average power absorbed from the wave by the first-stage energy conversion system and the absorbed power could be calculated according to the formula below based on the measured torque and pivoted angles,

$$P_{pto} = \frac{\sum_{t_o}^{t_f}\left(\Delta\theta \times \overline{T_{0.02}}\right)}{t_f - t_o} \tag{7}$$

where P_{pto} is average capture power, $\Delta\theta$ is the rotational angle in the period of 0.02 s, $\overline{T_{0.02}}$ is the average PTO damping torque in the period of 0.02 s.

The capture width ratio (CWR) η is an important indicator to evaluate the hydrodynamic efficiency of WECs (Budal and Falnes, 1975). The Stokes 2nd-order theory is used to obtain the incident wave power which is a more accurate representation of the recorded surface elevation for the waves considered in the present experiments. The incident wave power is a direct function of wave height H and the wave group celerity c_g (Flocard and Finnigan, 2010).

$$\eta = \frac{P_{pto}}{P_w D} \tag{8}$$

$$P_w = \frac{\rho g H^2 c_g}{8} \tag{9}$$

$$c_g = \frac{c}{2}\left(1 + \frac{2kh}{\sinh 2kh}\right) \tag{10}$$

where k is the wave number, P_w is the incident wave power per wave length, c is the incident wave velocity.

$$c = \frac{\omega_1}{k} \tag{11}$$

and the angular frequency ω_1 (i.e., *in the steady case, it is the same to the frequency of pitch motion of the flap in regular waves*) satisfies the following dispersion relation.

$$\omega_1^2 = gk\tanh kh \tag{12}$$

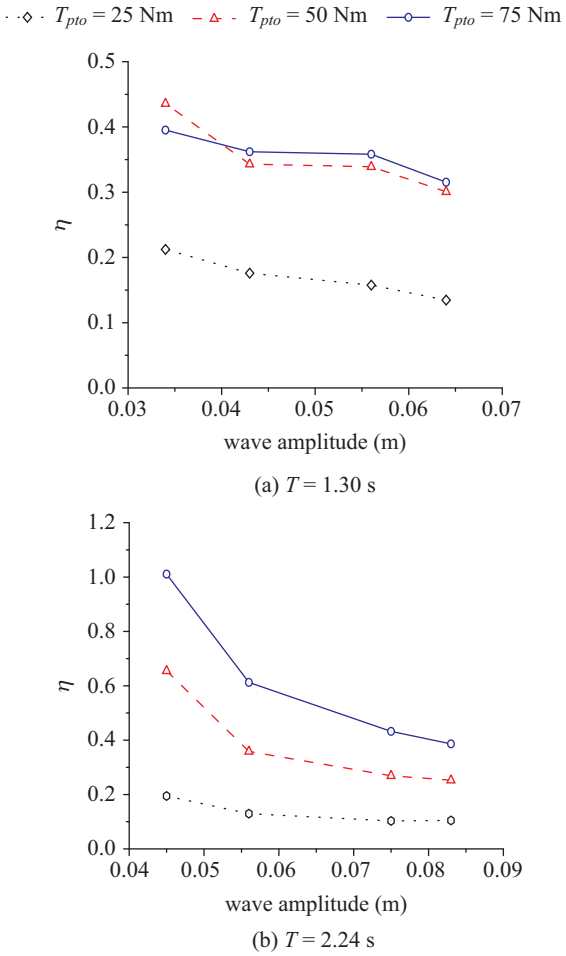

Fig. 5. Variations of capture width ratio η *vs* wave amplitude for different damping torque.

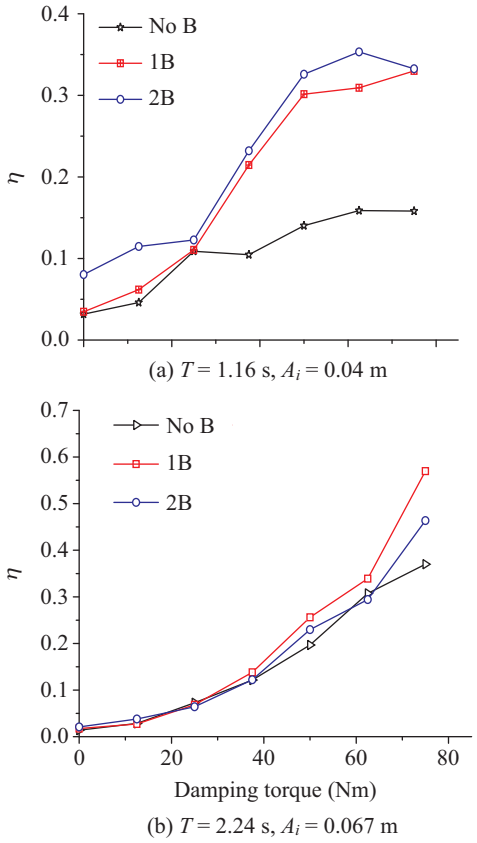

Fig. 6. Variations of capture width ratio η for different mass distribution (No B, 1B, 2B).

IV. RESULTS AND DISCUSSIONS

1. Performance of WEC Device in Regular Waves

The influences of the PTO damping torque, wave amplitude and mass distribution on the hydrodynamic performance are experimentally studied in this section. The water depth $h = 0.9$ m is used in this section if no otherwise is specified.

Fig. 5 presents the variations of the capture width ratio as the function of the incident wave amplitude for different damping torque. It can be seen that the capture width ratio decreases with increasing wave amplitude, which may be due to the viscous dissipation caused by vortex shedding and wave nonlinearity increasing with the increase of wave amplitudes. (Caska and Finnigan, 2008) also stated the same conclusions. They explained that wave amplitude dose not appreciably change the moment arm of the excitation force at least within the assumptions of linear wave theory, and the viscous effects also attributes to the decrease in capture width ratio with wave amplitude. Such decreasing trend is more apparent in the case of the larger damping torque.

To illustrate the effect of mass distribution on the hydrodynamic performance of the device, tests are conducted with three different mass distribution (i.e., *No B, 1B, 2B*) for two typical incident waves at $T = 1.16$ s, $A_i = 0.04$ m and $T = 2.24$ s, $A_i = 0.067$ m, respectively. From Fig. 6, it can be seen that different mass distributions have a significant effect on the performance of the OWSC device and it has a better performance in the case of 2B for short wave, whereas the plate in the case of 1B has a better performance for long wave.

Fig. 7 shows the time series of the flap rotation with three mass distribution (i.e., *No B, 1B, 2B*) for two typical incident waves at $T = 1.79$ s, $A_i = 0.083$ m and $T = 3.13$ s, $A_i = 0.067$ m, respectively. In the case of No B, the rotation response is bigger than the other two cases. Due to water ballast in the chambers, the rotation response of the model decreases. Then the viscous dissipation caused by vortex shedding and nonlinearity of waves also decreases.

Filling water to change the mass center can result in two distinct effects, i.e., the modification of the inertia moment I_1 and the change in the hydrostatic restoring coefficient C (Gomes et al., 2015). From Table 1, we can see that the natural period of the plate is 4.2 s for the No B case, 4.8 s for the 1B case, and 5.8 s for the 2B case. By filling water ballast, the mass center of the plate decreases, and the OWSC device has a relatively better performance compares with the No B case. The modification of inertia due to the filling water results in the changes of the location of the center of gravity, the pitching mass mo-

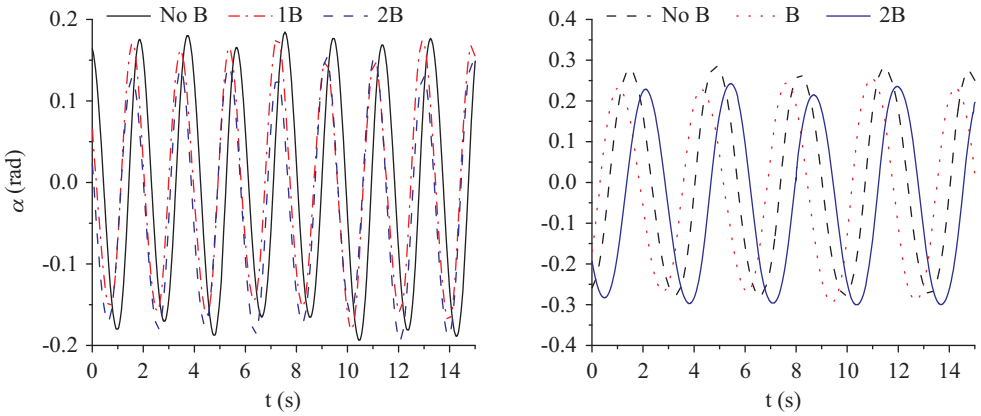

(a) $T = 1.79$ s, $A_i = 0.083$ m (b) $T = 3.13$ s, $A_i = 0.067$ m

Fig. 7. Comparison of the flap rotation angle α with damping torque $T_{pto} = 75$ Nm.

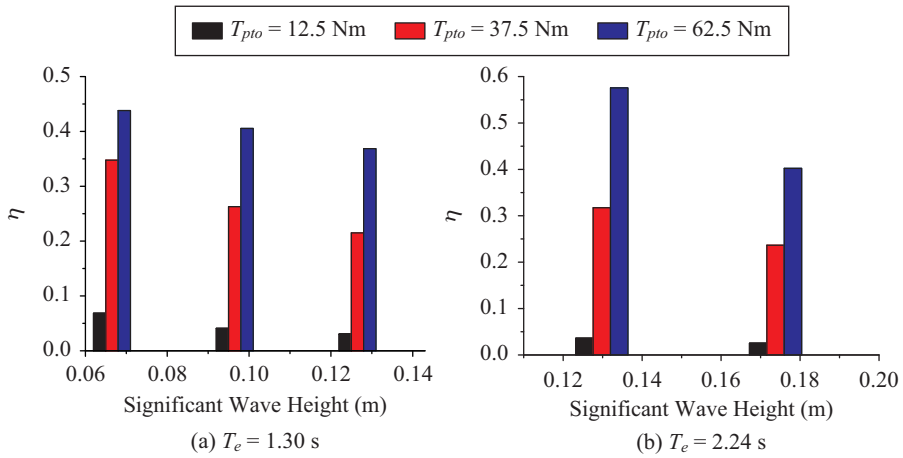

(a) $T_e = 1.30$ s (b) $T_e = 2.24$ s

Fig. 8. Variations of capture width ratio η *vs* significant wave height with JONSWAP spectrum.

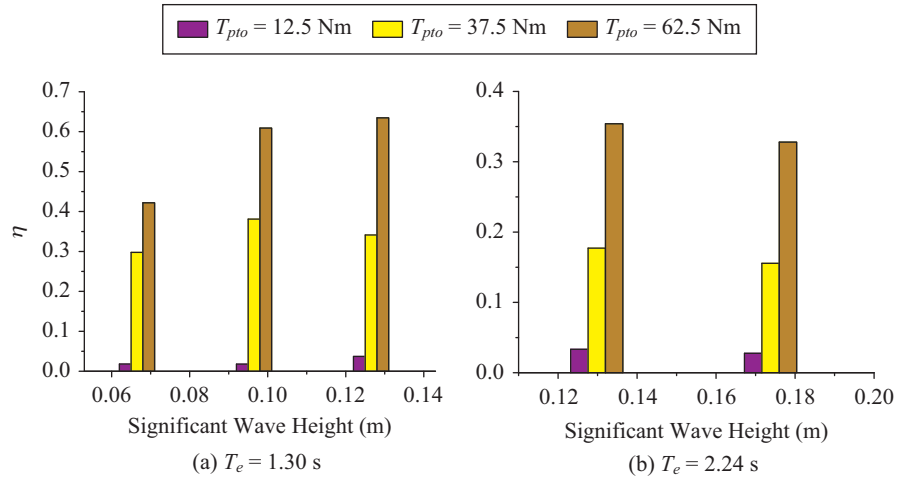

(a) $T_e = 1.30$ s (b) $T_e = 2.24$ s

Fig. 9. Variations of capture width ratio η *vs* significant wave height with PM spectrum.

ment inertia and the natural period. Moreover, the concept of adaptive filling water allows for an optimization of the performance of the device when wave climate evolves from the calm weather to the extreme conditions, while the device is prepared for a survival mode if necessary. If the weather which can potentially damage or destroy the device is predicted, the inertia

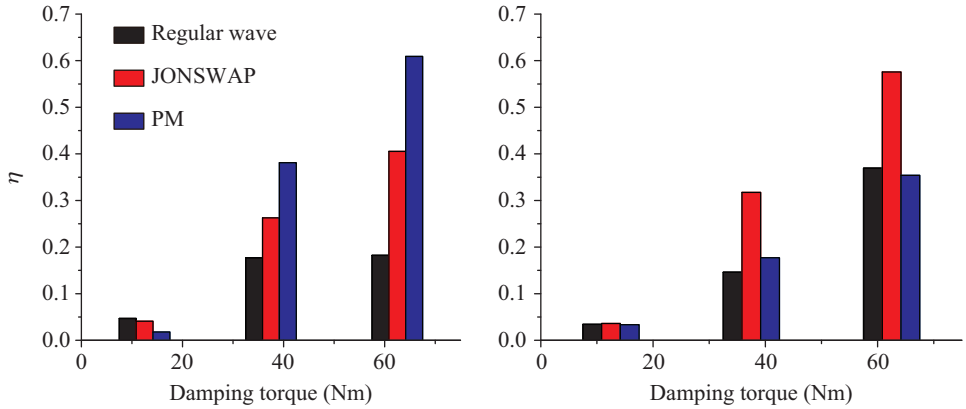

(a) T_e = 1.30 s, H_s = 0.10 m (b) T_e = 2.24 s, H_s = 0.134 m

Fig. 10. Variations of capture width ratio η *vs* damping torque for regular waves and irregular waves.

modification process can be carried on by completely ballasting the device and letting it sink to a horizontal position close to sea floor, where it will be protected (Flocard and Finnigan, 2012).

2. Results in Irregular Waves

It is also important to study the behavior and power output of wave energy devices in irregular waves as these better represent the real ocean conditions. Because JONSWAP and PM spectra are often considered in the ocean wave energy studies (Meadowcroft et al., 2005), they are also considered in this study. In order to estimate the power capture in irregular waves more realistically, each irregular wave train is generated with three times. Power capture for each irregular wave train is then averaged over these three different times.

The incident wave power in the irregular wave field over one meter wave front is expressed as:

$$P_w = \rho g \int_0^\infty C_g(\omega) S_B(\omega) d\omega, \tag{13}$$

where g is the acceleration due to gravity, $C_g(\omega)$ the wave group velocity, and $S_B(\omega)$ the maximum energy spectral density. The equation of the incident wave power can be simplified as the following form:

$$P_w = \frac{\rho g^2 H_s^{\,2} T_e}{64\pi}, \tag{14}$$

where T_e is the average wave period and H_s is the significant wave height (Flocard and Finnigan, 2010).

To illustrate the effect of different irregular wave spectra on the hydrodynamic performance of the device, tests are conducted with JONSWAP and PM spectra irregular waves for two typical incident waves at T_e = 2.24 s and T_e =1.30 s, respectively. Figs. 8-9 show the variations of capture width ratio with significant wave height for JONSWAP and PM spectra. The capture width ratio decreases with the increase of significant wave height while it increases with increasing damping torque in the case of JONSWAP spectrum, which is same to the above regular wave cases. However, there exists a critical significant wave height at which the capture width ratio reaches the maximum in the case of PM spectrum as shown in Fig. 9(a). (Ning et al., 2015; Ning et al., 2016) ever reported the same phenomenon for the OWC wave energy converter.

To illustrate the effect of different wave states on the hydrodynamic performance of the device, tests are conducted with regular waves, JONSWAP irregular waves and PM irregular waves for two typical incident waves at T_e = 1.30 s, H_s = 0.10 m and T_e = 2.24 s, H_s = 0.134 m, respectively. It can be seen that the capture width ratios all increase with the increasing damping torque and the converter has a better performance under the case of PM irregular waves for short wave as shown in Fig. 10(a). For long wave, the capture width ratio also increases with increasing magnetizing current, but the converter has a better performance for JONSWAP irregular waves as shown in Fig. 10(b). In summary, the wave state has a significant effect on the performance of the device. Above all, the OWSC performs better in irregular waves than in regular waves. The reason may be that the oscillation of the device is not at the resonance status in the condition of the regular wave. However, for irregular waves, there exist wave components more close to the natural oscillation frequency of the OWSC. This can be the reason why the OWSC performs better in irregular waves in this case. Still, it should be noted that this phenomenon may not be true when the regular wave is right at the natural frequency of the device.

V. CONCLUSIONS

In the present work, the hydrodynamic performance of a bottom-hinged flap-type device is experimentally investigated. The rationality of the experiment arrangement is verified through uncertainty analysis for the experimental results. The effects of PTO damping torque, wave amplitude and mass distribution on the hydrodynamic performance were examined. In addition, the effect of wave state on the hydrodynamic performance is also considered.

The PTO damping torque has strong influence on the hydrodynamic performance and the capture width ratio (CWR) increases with the PTO damping torque. The CWR decreases with the increase of the regular wave amplitude and the significant wave height for JONSWAP spectrum. In addition, the capture width ratio can be increased by filling water ballast into the OWSC device. From the comparison between the case of No B and 2B, it shows that, through filling water in the bottom two chambers, it can raise approximately 25% in power capture for the case of $T = 2.24$ s, $A_i = 0.067$ m, and $T_{pto} = 75$ Nm, and 20% for the case of $T = 1.16$ s, $A_i = 0.04$ m and $T_{pto} = 75$ Nm. The wave state is also an important factor to the hydrodynamic performance, i.e., higher CWR obtained easily in the environments of PM short waves and JONSWAP long waves, respectively. The reason may be due to that the energy density of the JONSWAP spectrum is more concentrated near the natural frequency of the OWSC than the PM spectrum. In summary, the incident wave parameters, different mass distributions and different spectrum all have significant effects on the performance of the flap-type OWSC device. The flap-type OWSC is a promising concept to exploit wave power in near-shore region, and the present investigation can be a guidance to assist in the safety analysis and site selection of the bottom-hinged flaptype OWSC devices. Besides that, it can also provide experimental data for validating numerical models.

ACKNOWLEDGEMENTS

The authors would like to gratefully acknowledge financial support from the National Science Foundation of China (Grant Nos. 51679036, 51490672) and Royal Academy of Engineering under the UK-China Industry Academia Partnership Programme (Grant No.UK-CIAPP\73).

APPENDIX

Fig. A. shows the time histories of the flap rotation angle α in the series of free decay tests with damping torque $T_{pto} = 0.0$ Nm for the cases of No B, 1B and 2B. From which the natural period of the OWSC device can be obtained for all the cases tested.

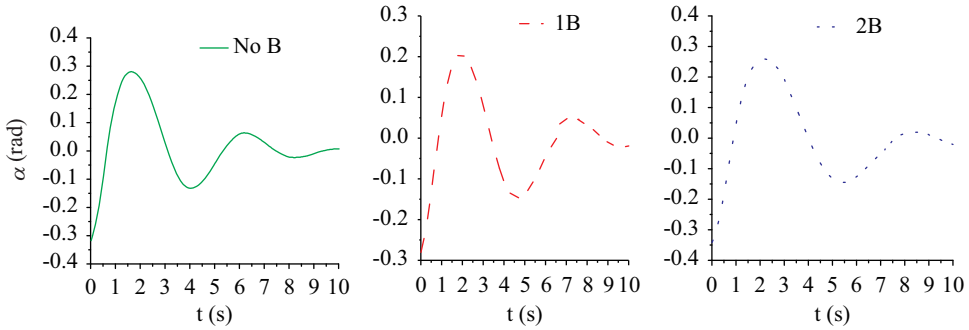

Fig. A. Time histories of the flap rotation angle α in the free decay tests.

Fig. B. shows the time histories of the wave elevation (i.e., *it is 1.7 m ahead of the device and is shown in Fig. 1*) for $T = 2.24$ s, $A_i = 0.067$ m and $T_{pto} = 75$ Nm, from which the measured wave amplitude A_i *and wave period* T are obtained as follows

$$A_i = \frac{A_{imax} - A_{imin}}{2}$$

$$T = \frac{T_u + T_d}{2}$$

where A_{imax} is the wave crest, A_{imin} is the wave trough. Here, A_{imax} *and* A_{imin} *are* adjacent to each other. In addition, T_u is the measured wave period by the method of the up crossing zero point, T_d is the measured wave period by the method of the down crossing zero point. From Fig. B, it can be seen that the measured wave period is 2.24 s while the wave amplitude is approximately 0.07m (i.e., *which is a little bigger than the input value 0.067m due to the reflection from the device*).

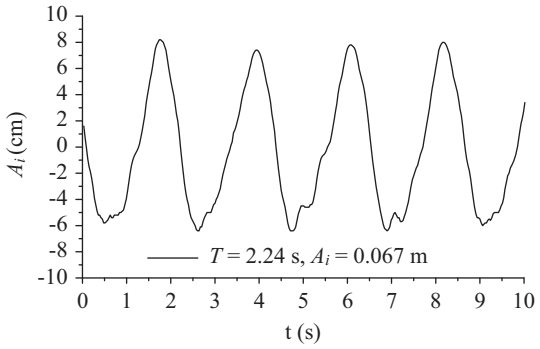

Fig. B. Time histories of wave elevation for T = 2.24 s, A_i = 0.067 m and T_{pto} = 75 Nm.

Fig. C. shows the time histories of damping torque T_{pto} *for the measured values and the Coulomb damping* with different magnetizing current for T = 3.13 s, A_i = 0.067 m.

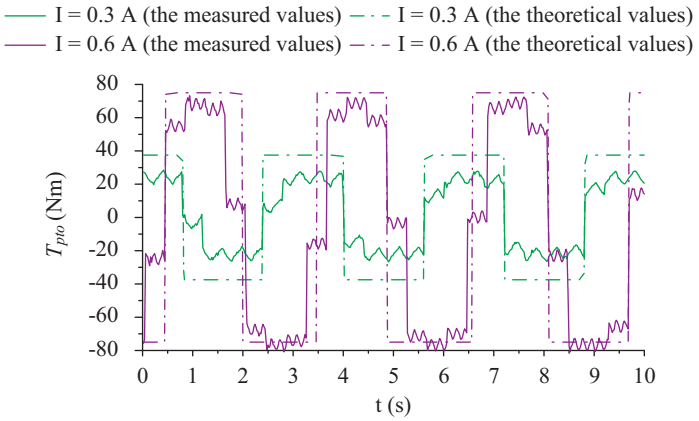

Fig. C. Time histories of damping torque T_{pto} for T = 3.13s, A_i = 0.067 m.

Fig. D. shows the time histories of the flap rotation angle α with damping torque T_{pto} = 75 Nm for T = 2.24 s, A_i = 0.067 m, from which the rotational response θ is obtained as follows

$$\theta = \frac{\alpha_{max} - \alpha_{min}}{2}$$

where α_{max} and α_{min} are the crest and trough value, respectively.

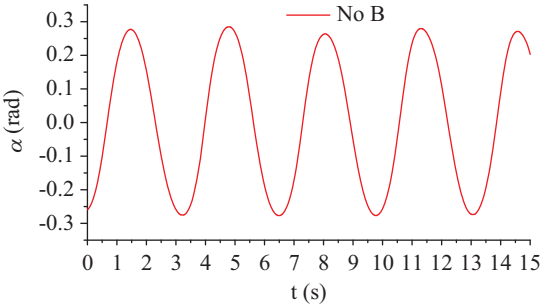

Fig. D. Time histories of the flap rotation angle α with T_{pto}=75 Nm at T = 3.13 s, A_i = 0.067 m.

Table A. Output damping torque of the magnetic powder brake system.

Magnetizing current (A)	0.1	0.2	0.3	0.4	0.5	0.6
The module value (Nm)	12.5	25	37.5	50	62.5	75

REFERENCES

Babarit, A., J. Hals, M. J. Muliawan, A. Kurniawan, T. Moan and J. Krokstad (2012). Numerical benchmarking study of a selection of wave energy converters. Renewable Energy 41(41), 44-63.

Budal, K and J. Falnes (1975). A resonant point absorber of ocean-wave power. Nature 256(5517), 478-479.

Caska, A. J. and T. D. Finnigan (2008). Hydrodynamic characteristics of a cylindrical bottom-pivoted wave energy absorber. Ocean Engineering 35(1), 6-16.

Clabby, D., A. Henry, M. Folley and T. Whittaker (2012). The effect of the spectral distribution of wave energy on the performance of a bottom hinged flap type wave energy converter. ASME 2012 31st International Conference on Ocean, Offshore and Arctic Engineering. American Society of Mechanical Engineers, 331-339.

Folley, M., T. J. T. Whittaker and A. Henry (2007a). The effect of water depth on the performance of a small surging wave energy converter. Ocean Engineering 34(8-9), 1265-1274.

Folley, M and T. J. T. Whittaker (2009). Analysis of the nearshore wave energy resource. Renewable Energy 34(7), 1709-1715.

Folley, M., B. Elsaesser and T. Whittaker (2009). Analysis of the wave energy resource at the European Marine Energy Centre. In Coasts, Marine Structures and Breakwaters CONF, Edinburgh, UK, September.

Folley, M., T. W. T. Whittaker and J. Van't Hoff (2007b). The design of small seabed-mounted bottom-hinged wave energy converters. Proceedings of the 7th European Wave and Tidal Energy Conference, Porto Portugal.

Fitzgerald, J and L. Bergdahl (2009). Rigid moorings in shallow water: A wave power application. Part I: Experimental verification of methods. Marine Structures 22(4), 809-835.

Flocard, F. and T. D. Finnigan (2010). Laboratory experiments on the power capture of pitching vertical cylinders in waves. Ocean Engineering 37(s 11-12), 989-997.

Flocard, F. and T. D. Finnigan (2012). Increasing power capture of a wave energy device by inertia adjustment. Applied Ocean Research 34(1), 126-134.

Gomes, R. P. F., M. F. P. Lopes, J. C. C. Henriques, L. M. C. Gato and A. F. O. Falcão (2015). The dynamics and power extraction of bottom-hinged plate wave energy converters in regular and irregular waves. Ocean Engineering 96, 86-99.

Hughes, S. A. (1996). Physical models and laboratory techniques in coastal engineering. Advanced (96), 588.

Meadowcroft, J., T. Stallard and N. Baker (2005). Comparison of power capture in irregular waves and their regular wave components. Proceedings of the 6th European Wave and Tidal Energy Conference, Glasgow, UK.

Ning, D. Z., J. Shi, Q. P. Zou and B. Teng (2015). Investigation of hydrodynamic performance of an OWC (oscillating water column) wave energy device using a fully nonlinear HOBEM (higher-order boundary element method). Energy 83, 177–188.

Ning, D. Z., R. Q. Wang, Q. P. Zou and B. Teng (2016). An experimental investigation of hydrodynamics of a fixed OWC Wave Energy Converter. Applied Energy 168, 636-648.

Penney, W. G. and A. T. Price (1952). Part I. The diffraction theory of sea waves and the shelter afforded by breakwaters. Royal Society of London Philosophical Transactions 244(882), 236-253.

Renzi, E. and F. Dias (2012). Resonant behavior of an oscillating wave energy converter in a channel. Journal of Fluid Mechanics 701(6), 482-510.

Renzi, E and F. Dias (2013). Hydrodynamics of the oscillating wave surge converter in the open ocean. European Journal of Mechanics - B/Fluids 41(3), 1-10.

Renzi, E., K. Doherty, A Henry and F. Dias (2014). How does Oyster work? The simple interpretation of Oyster mathematics. European Journal of Mechanics - B/Fluids 47(5), 124-131.

Sheng, W., R. Alcorn and A. Lewis (2015). Optimising power take-offs for maximizing wave energy conversions. The 30th International Workshop on Water Waves and Floating Bodies, Bristol, UK.

Saulnier, J., P. Ricci, M. Pontes and A. F. O. Falcao (2007). Spectral bandwidth and WEC performance assessment. Proceedings of the Seventh European Wave and Tidal Energy Conference, Porto Portugal.

Sarkar, D., E. Renzi and F. Dias (2013). Wave power extraction by an oscillating wave surge converter in random seas. ASME 2013 32nd International Conference on Ocean, Offshore and Arctic Engineering. American Society of Mechanical Engineers, V008T09A008.

Whittaker, T. and M. Folley (2012). Nearshore oscillating wave surge converters and the development of Oyster. Philosophical Transactions of the Royal Society A Mathematical Physical & Engineering Sciences 370(1959), 345-364.

Wei, Y., A. Rafiee, A. Henry and F. Dias (2015). Wave interaction with an oscillating wave surge converter, Part I: Viscous effects. Ocean Engineering 104, 185-203.

Wei, Y., T. Abadie, A. Henry and F. Dias (2016). Wave interaction with an oscillating wave surge converter, Part II: Slamming. Ocean Engineering 113, 319-334.